

Non-uniformity effects of the inter-foil distance on GEM detector performance^{*}

Yan Huang (黄彦)¹ Han YI(易晗)¹ Zhi-Gang Xiao(肖志刚)^{1,2;1)} Zhao Zhang(张钊)¹
 Wen-Jing Cheng(程文静)¹ Li-Ming Lü(吕黎明)¹ Wei-Hua Yan(闫威华)¹ Ren-Sheng Wang(王仁生)¹
 Hong-Jie Li(李红洁)¹ Yan Zhang(张嫣)¹ Li-Min Duan(段利敏)³ Rong-Jiang Hu(胡荣江)³
 Chen-Gui Lu(鲁辰桂)³ He-Run Yang(杨贺润)³ Peng Ma(马朋)³ Hai-Yan Gao(高海燕)^{1,4,5}

¹ Department of Physics, Tsinghua University, Beijing 100084, China

² Collaborative Innovation Center of Quantum Matter, Beijing 100084, China

³ Institute of Modern Physics, Chinese Academy of Sciences, Lanzhou 730000, China

⁴ Department of Physics and Triangle Universities Nuclear Laboratory, Duke University, Durham, NC 27708, U.S.A.

⁵ Duke Kunshan University, Kunshan, Jiangsu 215316, China

Abstract: The non-uniformity effect of the inter-foil distance has been studied using a gaseous electron multiplication (GEM) detector with sensitive area of 50mm×50mm. A gradient of the inter-foil distance is introduced by using spacers with different heights at the two ends of the foil gap. While the cluster size and the intrinsic spatial resolution show insignificant dependence on the inter-foil distance, the gain exhibits an approximately linear dependence on the inter-foil distance. From the slope, a quantitative relationship between the change of the inter-foil distance and the change of the gain is derived, which can be used as a method to evaluate the non-uniformity of the foil gap in the application of large-area GEM detectors.

Keywords: gaseous electron multiplication, non-uniformity effects, spatial resolution

PACS: 29.40.Gx, 29.40.Cs **DOI:** 10.1088/1674-1137/40/4/046001

1 Introduction

Since their advent in 1997 [1], the gaseous electron multiplication (GEM) detectors have been widely used in nuclear and particle experiments around the world for their high event rate capability and high spatial resolution [2–9]. Larger area planar GEM detectors have also recently installed or proposed in some experiments [10–17] to measure charged particle tracks. For the application of larger-area GEM detectors, many factors, such as gas mixture [18] and induction gap thickness [19], may have significant influence on the detector performance. In addition, two more factors have to be considered with care. One is the uniformity of the inter-foil distance. Due to force inhomogeneity in the extension of the foil, or the mutual electromagnetic force experienced by neighboring foils during operation, the surface of the foil may distort slightly and cause some non-uniformity in the inter-foil distance, which in turn affects the performance of the detector. Since the foil gap is usually smaller than the drift length of the initially-produced electrons, the inhomogeneity of the foil gap thickness may significantly affect the GEM detector performance and has to be studied in detail. Some fine spacers have been invented to keep a uniform inter-foil distance to stabilize the performance of large GEM detectors. The other factor is the strip width and inter-strip distance. A larger width and inter-strip distance helps to reduce the number of channels and effectively lower the cost, but may reduce the position resolution. In applications with low hit multiplicity, the delay line method has been applied to measure the hit position with rather high resolution [20].

In this paper, we invent a new method to study the non-uniformity effect of the inter-foil distance using a small area GEM detector, and the influence of the inter strip distance on spatial resolution is also investigated by comparing the detector performance with different strip dimensions. The paper is arranged as follows. In Section 2 the experimental setup and the method for the non-uniformity studies is introduced. Section 3 presents the performance of the GEM detector, the non-uniformity effects of the inter-foil gap thickness and the spatial re-

Received 23 April 2015

^{*} Supported by National Natural Science Foundation of China (11375094, U1332207, 11120101004), and by Tsinghua University Initiative Scientific Research Program

1) E-mail: xiaozg@tsinghua.edu.cn

©2016 Chinese Physical Society and the Institute of High Energy Physics of the Chinese Academy of Sciences and the Institute of Modern Physics of the Chinese Academy of Sciences and IOP Publishing Ltd

solution with different readout strips. A summary is given in Section 4.

2 Experimental setup

A planar GEM detector prototype with two GEM foils made at CERN was assembled for the test. The sensitive area of the GEM foil was $50 \times 50 \text{ mm}^2$. Both the drift length above the upper GEM foil and the induction gap below the lower GEM foil were 3 mm. The initial inter-GEM distance was 2.2 mm. The working gas in this test was a mixture of argon and CO_2 in 85% and 15% mass proportion, respectively, unless otherwise specified. To get collimated incident X-rays, an aluminum slit with adjustable width from about 0 to $2000 \mu\text{m}$ was installed approximately 4 mm above the Mylar window of the GEM detector. The thickness of the slit was 5 mm. The slit was fixed on a platform which was precisely movable in one of the horizontal directions, along which the gradient of the inter-foil gap thickness could be introduced in the test. This direction is defined as x throughout text. An Fe-55 source with approximately $5 \times 10^4 \text{ Bq}$ activity was used in the experiment. A schematic view of the experimental test in the direction perpendicular to the readout strips is depicted in Fig. 1(a).

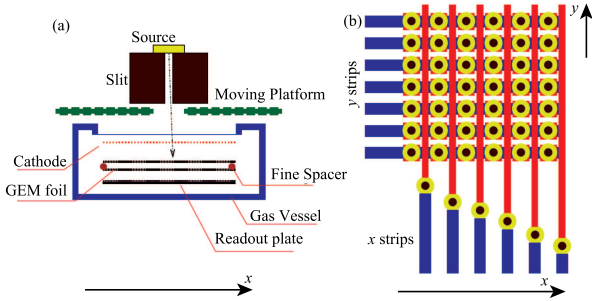


Fig. 1. (color online) (a) Schematic view of the experimental setup and (b) the pattern of the readout strips. The slit was mounted on a precisely movable platform moving along the x axis. The spacers between the GEM foils could be finely adjusted to introduce non-uniform gap thickness along the x axis. The strip-to-strip distance of $x(y)$ strips was $446 (625) \mu\text{m}$. The strip width was $125 (345) \mu\text{m}$ for $x(y)$ strips. The radius of the holes was $150 \mu\text{m}$. For clearer display, the components are not shown to scale.

The two dimensional strip readout pattern is presented in Fig. 1 (b). The sensitive readout range is 50 mm in both x and y directions. Here we define the strips which are in parallel with the y axis as x strips since they deliver the hit position along the x direction using the centroid method, while the y strips are in parallel with the x axis and can give the hit position along the y direction, as depicted in Fig. 1 (b). By this definition, there

are $7 \times 16 x$ strips and $5 \times 16 y$ strips within the sensitive area. The inter-strip distances are 446 and $625 \mu\text{m}$ for x and y strips, respectively. The induced signals are read out by a CASAGEM board based on ASIC technology. Each board has one ASIC chip which can handle 16 signal channels. The chip provides the amplification and the shaping of the input signal [21]. The performance of the ASIC chip is summarized in Table 1. The response of the CASAGEM amplifier and the analog-digit converter (ADC) is calibrated using a precise pulse generator.

Table 1. The specifications of the CASAGEM board.

parameter	value
gain	2 – 40mV/fC
dynamic range	0 – 1000 fC
shaping time	20 – 80 ns
INL	< 1%
POWER	< 11 mW/ch
ENC	< 3000e

3 Results and discussion

3.1 Energy and spatial resolution of the GEM detector

We first check the general performance of the detector, i.e., the energy resolution and spatial resolution of the detector before introducing the extra spacer to vary the inter-foil distance. Figure 2 (a) and (b) presents the energy spectrum detected on the x and y strips, respectively. It is shown that the position of the full energy peak of the Fe-55 source differs in the x and y directions, given that the electronics have been calibrated. This difference is attributed to the structure of the readout board. In the current design, the gold-coated sensitive area is different for x and y strips. It turns out that the ratio of the signal height is approximately proportional to the gold-coated area that collects the induction

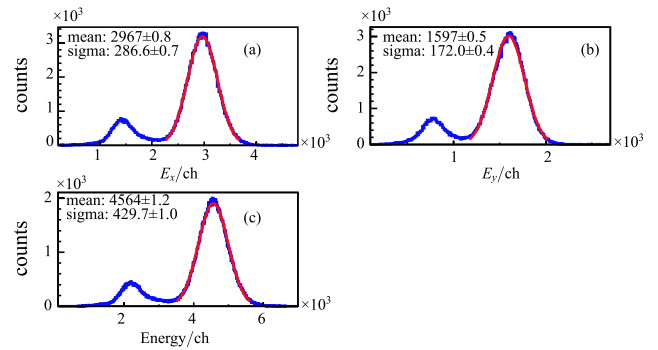


Fig. 2. (color online) Energy spectra recorded with (a) x , (b) y strips and (c) the sum over x and y directions.

charge. The solid curves in the three panels represent the Gaussian fit to the main peak. The relative energy resolution of E_x is 22%, slightly better than E_y due to the larger amplitude. It is believed that the size of the holes on the y strips may reduce the charge collected and hence the energy resolution. The total energy spectrum E_{tot} , as plotted in panel (c), has an energy resolution of 22%. The resolution of the total energy signal E_{tot} is slightly better than E_x and E_y because the total signal collects more charge than either E_x or E_y .

The spatial resolution can be obtained from the position distribution since the incident X-ray is well collimated by the slit. The position of x (or y) for each event is calculated from the centroid of the fired strips. Since the strip width is of the order of hundreds of micrometers, more than one (usually) neighboring strips will be fired in each event for a single incident particle, and the signals on adjacent strips are correlated. The broadening of position distribution along the normal direction of the slit includes the contributions from the intrinsic spatial resolution as well as from the finite width effect of the slit. The spatial resolution analysis is based on the events that fill in the full energy peak cut, as depicted in Fig. 3 (a). Figure 3 (b) is the raw two dimensional position distribution. The two dimensional distribution is then rotated upright and projected onto the normal axis of the slit, as shown in panels (b) and (c) respectively. A Gaussian fit is adopted to extract the total variance of the position distribution, as depicted in panel (d).

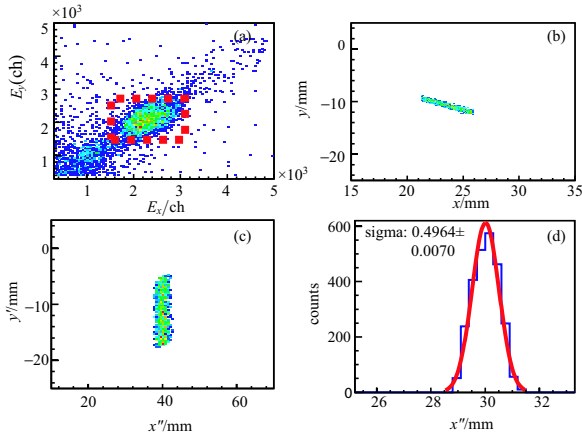


Fig. 3. (color online) (a) The correlation scattering plot of x and y directions; the imaging of the slit (b) before and (c) after rotating to the upright orientation; and (d) the projection of the position distribution along the slit.

In order to subtract the contribution from the finite slit width and obtain the intrinsic spatial resolution of the detector, a practical method was invented in our previous work and is used here [22]. It has been found that the event rate n is proportional to the square of the slit

width w^2 , reflecting the broadening of the position distribution due to the finite slit width, i.e., $n \propto w^2 \propto \sigma_w^2$. Hence, the total variance of the position distribution is expressed by $\sigma_{\text{tot}}^2 = \sigma_{\text{gem}}^2 + cn$, where σ_{gem} is the intrinsic spatial resolution of the GEM detector and c is a constant depending on the setup geometry. Figure 4 shows the values of σ_{tot}^2 as a function of the counting rate of the full energy peak under different experimental geometric conditions. In panel (a), the slit is placed above the GEM detector and at an angle of about 45° with respect to the x strips. In panel (b), the slit is parallel to the y strips. Through the intercept of the linear fitting to each data set, one can derive the intrinsic spatial resolution of the GEM detector under the corresponding geometric condition. Table 2 summarizes the intrinsic spatial resolution results with the experimental uncertainty (1σ). The inter-strip distance d normalized to $\sqrt{12}$ (assuming a uniform distribution of the incident position within the gap of two neighboring strips) is also presented. For the results in row (a) corresponding to the measurement in panel (a) in Fig 4, the inter-strip distances in both x and y directions have to be taken into account by

$$d = \sqrt{(k^2 d_x^2 + d_y^2) / (1 + k^2)}, \quad (1)$$

where k is the slope parameter of the slit with respect to the x axis. It is then clear that k measures the angle between the slit and the x strip. For instance, with $k = 0$, the slit is parallel with the y strips and the resolution is determined by the distance between two neighboring y strips. The last row of the table is the result obtained with a single dimensional readout strip, where the intrinsic spatial resolution is comparable to the inter-strip distance divided by $\sqrt{12}$ on the readout board. The factor $\sqrt{12}$ is introduced assuming the incident position follows a uniform distribution in the gap between two stripes. In the present two dimensional measurement, the intrinsic resolution deviates slightly from the prediction of $d/\sqrt{12}$. It indicates that the current design of the two dimensional readout strip may deteriorate position resolution, possibly because the coverage of the conductive induction surface in both directions is low and part of the y strips are buried under PCB materials, as shown in Fig. 1(b).

Table 2. The position resolution at different strip conditions.

strip width / μm	$\sigma_{\text{exp}}/\mu\text{m}$	$d/\sqrt{12}/\mu\text{m}$
$d_x(d_y) = 446(625)$	204 ± 13	160
$d_x = 446$	159 ± 22	129
$d_x = 200$	56 ± 15 [22]	58

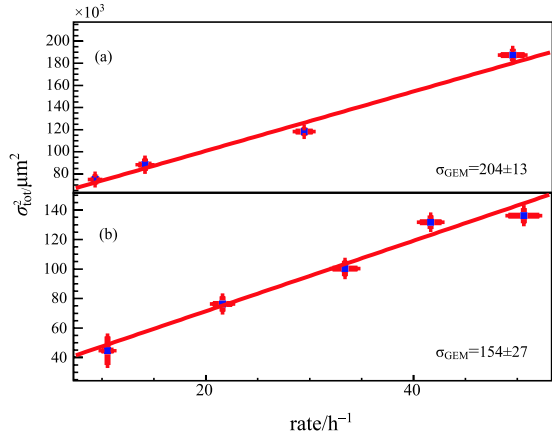


Fig. 4. (color online) The total variance of the position distribution in two configurations: (a) the slit is at about 45° to the x strips and (b) the slit is parallel to the x strips.

3.2 Non-uniformity effect of the inter-foil distance

In order to investigate the non-uniformity effect of the inter-foil distance, two extra spacers were used at two ends between the GEM frames to form a wedge-shaped inter-foil space along the x direction. Thus, the inter-foil distance increases with x position, while along the y direction the inter-foil distance keeps constant at a given x . Figure 5 shows a schematic view of the non-uniform inter foil gap. Two configurations were tested using two types of extra spacers with different heights. The central distance l_0 and the height of the spacers at both ends of the x direction, l_1 and l_2 , are listed in Table 3.

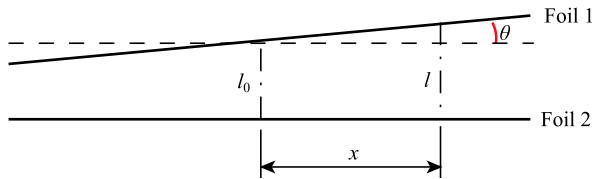


Fig. 5. (color online) Schematic view of the tilting of the GEM foil. For clarity only the upper foil is tilted by a finite angle θ ; the length quantities are shown in the figure.

Table 3. The experimental parameters in the inter-foil distance inhomogeneity test.

	l_0/mm	l_1/mm	l_2/mm	dl/dx
C_1	2.9	2.3	3.5	0.020
C_2	2.3	1.2	3.4	0.036

Figure 6 presents the full energy peak position (FEPP) of the Fe-55 source as a function of the x position with configuration C_2 at given settings of the gas mixture and working voltages as indicated in the figure. The voltage varies from 1710 to 1990 V while the argon concentration varies from 75% to 90%. For reference, the FEPP

measured before introducing the wedge-shaped foil gap is also plotted. It is shown that the channel position of the full energy peak, which reflects the relative gain of the detector, keeps nearly constant along the x direction when there is no non-uniformity in the gap thickness, as well as along the y direction, for which the gap is not changed. When the inter foil distance is changed, however, the FEPP exhibits an evident systematic trend. With increasing gap thickness along the x direction, the FEPP decreases constantly in the sensitive area. The slope of the FEPP distribution is nearly identical for all the gas mixtures and working voltages.

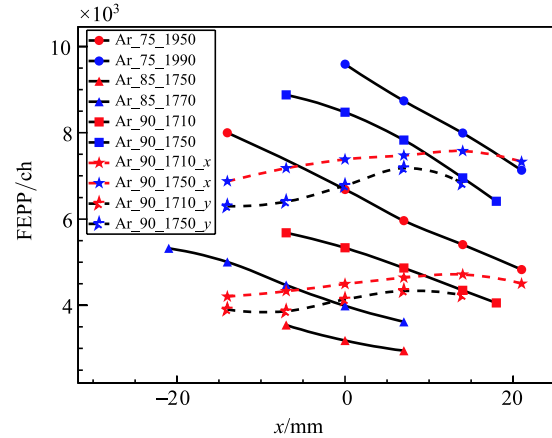


Fig. 6. (color online) Channel position of the Fe-55 source full energy peak as a function of incident position. The dashed curves connecting the symbols denote the results without introducing the non-uniformity of the gap thickness, while the solid curves are the results with configuration C_2 at various gas mixtures and working voltages.

Figure 7 (a) presents the full energy peak position (FEPP) at different incident positions with the two geometric configurations C_1 and C_2 . The FEPP decreases with increasing the inter-foil distance and exhibits a difference between the two configurations. In the first setup, C_1 , the decreasing rate of the gain represented by FEPP as a function of distance is smaller because the inter-foil distance changes less rapidly. If we check the relative gain (FEPP normalized to the value at the center) as a function of the relative change of the inter-foil distance l/l_0 , as plotted in panel (b), it is interesting to notice that the data points in the two setups merge approximately to the same line with an identical slope, which implies that the gain is indeed sensitive to the relative change of the foil gap thickness, but not to how fast the change of foil gap is formed in the application of large GEM detectors. From the slope value, it is shown that if the gap thickness changes by 1%, the gain changes approximately by $(1.00 \pm 0.09)\%$. This correspondence, robust against the change of the gas mixtures, the working voltage and the angle of the wedge shape foil gap,

establishes a quantitative relation between the uniformity of the inter-foil distance and the variation of the average gain of the detector, and offers a new method to evaluate the foil distortion and the uniformity of the foil gap in real application of larger area GEM detectors.

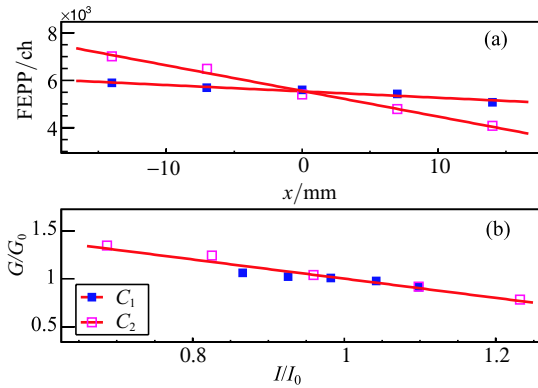


Fig. 7. (color online) The gain, represented by the channel of the full energy peak, (a) as a function of the incident position of the Fe-55 X-rays and (b) as a function of the gap thickness normalized to the thickness at the central point.

Figure 8 presents the distributions of multiplicity of the fired strips (a) and cluster size (b) at different incident positions. The cluster size is defined as the standard deviation of the signal height distribution in each individual event by

$$E = \frac{\sum a_i (x_i - \bar{x})^2}{\sum a_i}, \quad (2)$$

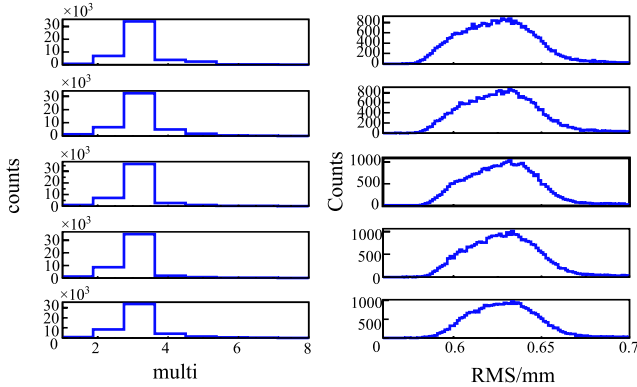


Fig. 8. (color online) (a) The multiplicity of the fired strips and (b) the root mean square (RMS) of the signals on neighboring strips in individual events.

where x_i and a_i are the position and the signal height, respectively, on the i^{th} strip. The sum is over the strips fired in the same event and \bar{x} denotes the position derived from the centroid of the fired strips. From the multiplicity distribution, it is shown that the number of

fired strips exhibits insignificant difference with changing inter-foil distance. Given the fact that the signal amplitude changes along the incident position due to the foil gap variation, but since the change is very small in the extension of the fired area in each single event, the variance of the signal distribution, the cluster size, is approximately constant. This implies that a slight inhomogeneity of the GEM foil gap will not cause a significant change in the position resolution.

To confirm the above assumption, Fig. 9 presents the total variance of the position resolution as a function of the event rate measured at two positions, $x = 0$ and 3 cm to the center of the detector in the C_2 configuration, with the GEM foil gap being $l = 1.2$ and 2.5 mm, respectively. By fitting the data points with a linear function, it is derived that the intrinsic position resolution at these two positions are $\sigma_1 = 154 \pm 27$ and $\sigma_2 = 167 \pm 18$ μm respectively. Within the uncertainty, the spatial resolution is the same at these two inter-foil distances.

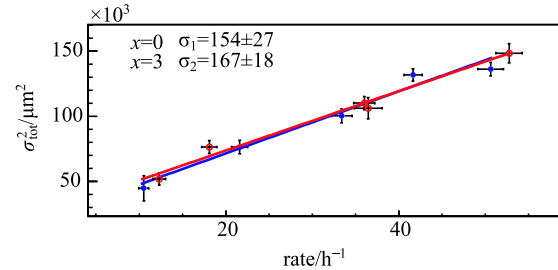


Fig. 9. (color online) The total variance of the position distributions measured at two incident positions in the C_2 configuration.

4 Summary

In summary, we describe a new method to investigate the non-uniformity effect of the inter-foil distance on the gain and spatial resolution of GEM detectors. Using a GEM detector prototype with a small sensitive area, for which the distortion of the GEM foil is negligible during assembly, we introduce a constant gradient to the gap thickness by placing different spacers on the ends between the two GEM foils. By measuring the performance at different incident positions, it is found that the gain exhibits an approximate linear dependence on the slight change of inter-foil distance, while the spatial resolution shows insignificant variation over the inter-foil distance. It is found in our setup that 1% variation of the inter-foil distance causes approximately $(1.00 \pm 0.09)\%$ variation of the gain parameter or the channel position of the full energy peak. This correspondence may provide a reference in the evaluation of foil inhomogeneity in real applications of large-area GEM detector. In addition, by measuring the spatial resolution with different configurations of the readout strips, it is found that the intrinsic

resolution is comparable to the inter-strip distance of the inducing readout board while a slight deterioration is visible because of the reduction of the inductive surface of the readout strips. This provides a reference for the readout design of large-area GEM detectors.

The authors would like to thank Dr. Rui de Oliveira from CERN for his support on GEM production and to Prof. Zhi Deng from the Department of Engineering Physics of THU for providing the CASAGEM board.

References

- 1 F. Sauli, Nucl. Instrum. Methods A, **386**: 531 (1997)
- 2 T. Barvich et al, Nucl. Instrum. Methods A, **485**: 477 (2002)
- 3 F. Simon et al, IEEE Trans. Nucl. Sci., **54**: 2646 (2007)
- 4 Y. L. Li et al, Nucl. Instrum. Methods A, **596**: 305 (2008)
- 5 V. M. Aulchenko et al, Nucl. Instrum. Methods A, **598**: 112 (2009)
- 6 F. Simon F et al, Nucl. Instrum. Methods A, **598**: 432 (2009)
- 7 P. Martinengo et al, Nucl. Instrum. Methods A, **604**: 8 (2009)
- 8 K. Fujita et al, Nucl. Instrum. Methods A, **608**: 48 (2009)
- 9 F. Murtas et al, Nucl. Instrum. Methods A, **617**: 237 (2010)
- 10 C. Altunbas et al, Nucl. Instrum. Methods A, **490**: 177 (2002)
- 11 B. Ketzer et al, Nucl. Instrum. Methods A, **535**: 314 (2004)
- 12 B. Surrow et al, Nucl. Instrum. Methods A, **617**: 196 (2010)
- 13 M. Alfonsi et al, Nucl. Instrum. Methods A, **617**: 151 (2010)
- 14 H. Y. Gao et al, Eur. Phys. J. Plus, **126**: 2 (2011)
- 15 K. Gnanvo et al, Nucl. Instrum. Methods A, **782**: 77 (2015)
- 16 S. Bachmann et al, Nucl. Instrum. Methods A, **438**: 376 (1999)
- 17 W. H. You et al, Chinese Physics C, **39**: 046001 (2015)
- 18 A. Orthen et al, Nucl. Instrum. Methods A, **512**: 476 (2003)
- 19 G. P. Guedes et al, Nucl. Instrum. Methods A, **497**: 305 (2003)
- 20 Y. Zhou et al, Nucl. Instrum. Methods A, **604**: 71 (2009)
- 21 L. He et al, in IEEE Nuclear Science Symposium and Medical Imaging Conference Record (NSS/MIC, 2012), P N14-16
- 22 R. S. Wang et al, Nucl. Instrum. Methods A, **701**: 54 (2013)